ISSN 1063-780X, Plasma Physics Reports, 2023, Vol. 49, No. 12, pp. 1501–1514. © Pleiades Publishing, Ltd., 2023.
Russian Text © The Author(s), 2023, published in Fizika Plazmy, 2023, Vol. 49, No. 12, pp. 1293–1307.

TOKAMAKS

Neutral Injection Complex for Globus-M2 Spherical Tokamak

P. B. Shchegolev[a],*, V. B. Minaev[a], A. Yu. Telnova[a], V. I. Varfolomeev[a], V. K. Gusev[a], L. A. Esipov[a], N. S. Zhiltsov[a], V. V. Kolmogorov[c], A. A. Kondakov[c], G. S. Kurskiev[a], I. V. Miroshnikov[a], A. A. Panasenkov[b], A. V. Sorokin[c], and I. A. Shikhovtsev[c]

[a] *Ioffe Institute, Russian Academy of Sciences, St. Petersburg, 194021 Russia*
[b] *National Research Center "Kurchatov Institute," Moscow, 123098 Russia*
[c] *Budker Institute of Nuclear Physics, Siberian Branch, Russian Academy of Sciences, Novosibirsk, 630090 Russia*
**e-mail: peter_shchegolev@mail.ioffe.ru*

Received July 15, 2023; revised September 18, 2023; accepted October 1, 2023

Abstract—The injection complex that heats plasma of Globus-M2 spherical tokamak consists of two injectors which supply high-energy beams of hydrogen (deuterium) atoms into the device's plasma. Injectors are autonomous and allow for preparing and setting up the device and measuring the parameters of the atomic beam independently of the other injector and of the tokamak. The authors provide detailed analysis of each injector's configuration, substantiate their selection of the experiment layout for introducing beams into the tokamak plasma, set forth characteristics of both injectors' atomic beams injected into the tokamak plasma, and discuss the results of experiments on additional heating of Globus-M2 tokamak plasma obtained by injecting two atomic beams.

Keywords: atomic injector, ion source, high-energy atomic beam, ion-optical system, neutral beam injection
DOI: 10.1134/S1063780X23601098

INTRODUCTION

Globus-M2 spherical tokamak (R = 0.36 m, a = 0.24 m, $B_t \le 1$ T, $I_p \le 0.5$ MA; where R is the major radius, a is the minor radius, B_t is the toroidal magnetic field, I_p is the plasma current) [1], is an upgraded version of the Globus-M device (R = 0.36 m, a = 0.24 m, $B_t \le 0.5$ T, $I_p \le 0.3$ MA) [2], which was equipped with one atomic injector (detailed description of Globus-M provided in [3]). In addition to increasing the toroidal magnetic field and plasma current, the Globus-M tokamak upgrade included the development of additional plasma heating systems, which involved improvements to the existing Neutral Beam Injector (NBI-1) and the installation of the second injector (NBI-2).

Injection of beams of fast atoms into the tokamak plasma has been widely used for additional heating and current drive. As a result of upgrading auxiliary plasma heating systems in the Globus-M2 tokamak, the injection of two neutral hydrogen or deuterium beams was implemented (particle energy for one injector up to 40 keV at up to 1 MW power; for the second injector up to 50 keV at up to 1 MW power) with a total output power up to 2 MW, which is several times higher than the power of ohmic heating. Injecting two beams of atoms into the device's plasma may help it achieve higher beta values close to the ideal limit (based on normalized beta).

To achieve maximum temperature of plasma and energy stored therein in tokamaks, it is much more efficient to input energy in ions because of the anomalously high thermal conductivity of electrons. Implementing the preferential ion heating at injection energies below the critical E_c value (approximately 40 keV for deuterium beam injection into hydrogen plasma at $\langle T_e \rangle = 1$ keV) [4] at the MW power level allows for a significant increase in the ion temperature T_i compared to the electron temperature T_e [5], thus coming near the range of experimental parameters typical of a thermonuclear reactor. In general, an additional channel for heating ions (besides their collisions with electrons) makes it possible to change the ratio of ion and electron temperatures over a wide range, which in itself is of great interest for the study of the T_i/T_e ratio's effect on the transfer of heat and particles in the ion and electron channels [6]. Moreover, injecting two atomic beams with different geometric sizes and spatial power density distribution into the plasma provides additional opportunities for optimizing the density of plasma current. In addition, the upgraded neutral injection complex of the Globus-M2 tokamak significantly expands the range of studies of fast ions and relevant MHD physics [7], as well of plasma rotation induced by them [8].

Table 1. Specifications of the NBI-2

Working gas	Hydrogen, deuterium
Accelerating voltage, kV	from 30 to 50
Maximum ion current for hydrogen, A	45
Maximum power of an atomic beam, MW	1
Emission surface size, mm	200
Beam diameter at the calorimeter (by power level of 1/*e*), mm	Not larger than 110
Maximum pulse duration, s	1
Pause between pulses of maximum duration, min	10
Beam divergence, degree	1.2
Focal length, m	3.5 ± 0.5

CONFIGURATION OF THE SECOND ATOMIC INJECTOR

The upgrade for the neutral injection complex of the Globus-M2 tokamak included the installation of NBI-2 [9], its technical characteristics provided in Table 1. Its design is based on an injector for plasma heating developed at the Institute of Nuclear Physics of the Siberian Branch of the Russian Academy of Sciences [10].

The NBI-2 is a platform-mounted vacuum chamber with a deflection magnet, neutralizer, passage diaphragm, ion dump, aiming device, and two cryopumps. An ion source is attached to one side of the chamber, and a movable absorbing calorimeter is mounted on other side. The NBI-2 also includes vacuum pumping, power supply, working gas puff, water cooling, control, and data acquisition systems that ensure its operations. The layout drawing of the injector is shown in Fig. 1.

The vacuum chamber of Injector *1* (volume ~2.5 m^3) is made of stainless steel 304L. The chamber is shaped as a rectangle with inner dimensions of 800 × 1680 × 1884 mm, 10 mm side walls, and stiffeners welded on the outside. A ∅540 mm port connecting Neutralizer *6* and Ion Source *4* is located on one side of the end wall, and a ∅690 mm port connecting the Calorimeter *10* is on the other side. Two 760 × 800 mm rectangular ports on top of the vacuum volume are used to mount Cryopumps *3*. A ∅200 mm Passage Diaphragm *7* is installed inside the chamber. The diaphragm cuts off the peripheral part of the beam and divides the volume into two parts to ensure higher vacuum on the calorimeter side. The injector chamber is installed on Platform *2* equipped with rollers, which allow for its movement along 2600 mm rails. It is provided with adjustable supports to adjust the position of the injector in the horizontal and vertical directions by ±10 mm.

The ion source (Fig. 2) consists of the Gas Discharge Chamber (GDC) *3*, wherein plasma emitter is created, and a three-electrode Ion-Optical System (IOS) *5*, which ensures the formation, acceleration, and focusing of the ion beam. The cylindrical part of the GDC (117 mm long, ∅296 mm) is made of ceramic (Al_2O_3). The water-cooled rear molybdenum flange of the GDC is outfitted with a set of permanent magnets whose field reduces the plasma flow onto the wall, thereby increasing the energy efficiency of the discharge. The inner surface of the ceramic chamber is protected from direct contact with plasma by a copper Faraday shield. The working gas is puffed to the GDC through Ignition Unit *2*, which is mounted in the center of the chamber's rear wall, by means of an electromagnetic pulse valve. The discharge is initiated by supplying high-voltage pulse with an amplitude of up to 6 kV between the valve body and the GDC rear flange insulated from it by a ceramic tube that contains the ignition electrode. A short spark which is formed along the inner surface of the ceramic tube is ejected into the plasma chamber where high-frequency discharge is ignited. It is excited at 4 MHz frequency using an external three-turn Antenna *4* made of copper tube, whereas high-frequency power is supplied to it through an oil-insulated isolation transformer. At 45 kW RF power absorbed in the GDC plasma, the emitter is capable of producing the ion current of up to 45 A (on hydrogen).

The extraction from the GDC plasma and the acceleration of positive ions is performed using an IOS which consists of three nested grids (∅200 mm) composed of hexagonally arranged holes having a circular aperture. The combination of the three grids' coaxial holes forms an IOS elementary cell, its geometry and dimensions shown in Fig. 3. The IOS grids are made in the shape of spherical segments, which ensures the overall beam focusing at a distance of 3.5 m from the ion source. The ion-optical injector system is optimized to produce a beam with the minimum angular divergence in the order of 0.9°. The IOS electrodes (the first made of molybdenum of TsM2A grade, the rest of chromium-zirconium bronze of BrKhTsr grade) are installed on copper ring flanges connected to each other using two ceramic Insulators *7*, their height being 80 and 10 mm, respectively. The first grid is 3.5 mm thick, and the second and third grids are

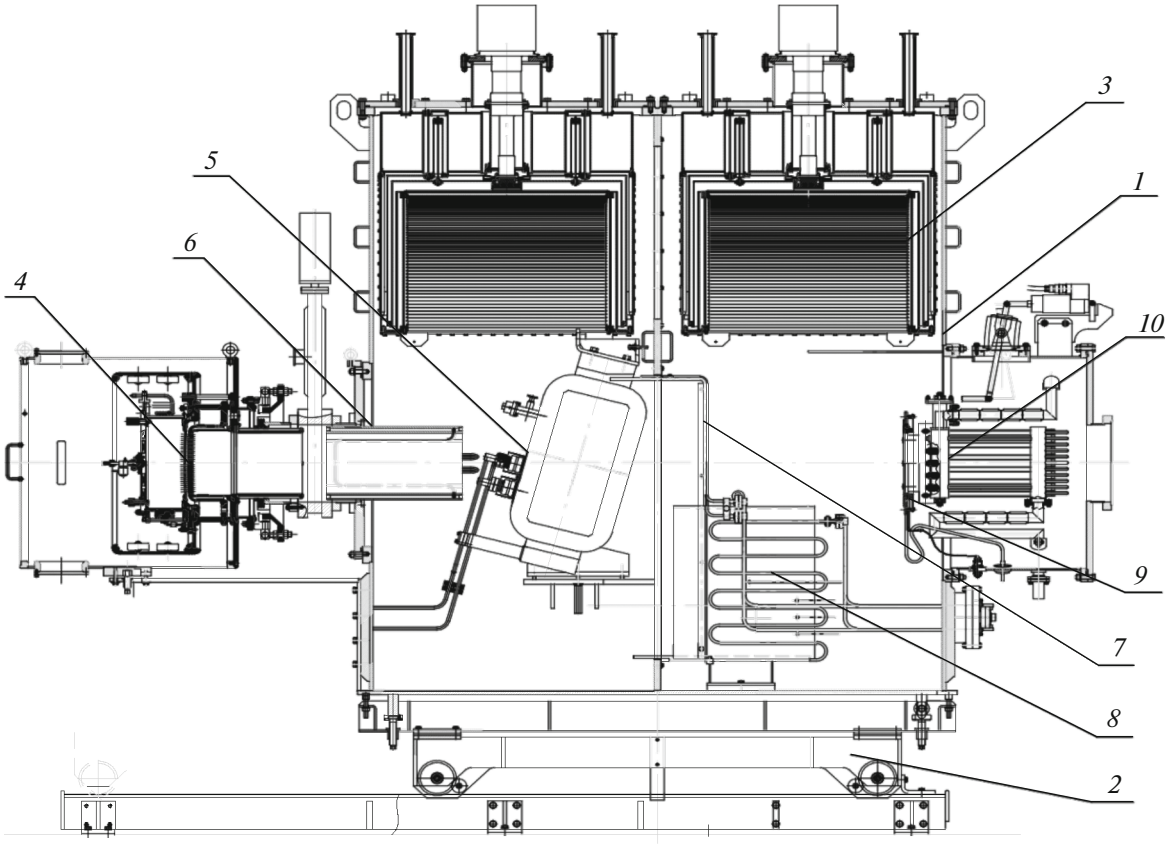

Fig. 1. Layout drawing of the NBI-2: (*1*) vacuum volume; (*2*) platform; (*3*) cryopump; (*4*) ion source; (*5*) deflection magnet; (*6*) neutralizer; (*7*) diaphragm; (*8*) ion dump; (*9*) aiming device; (*10*) calorimeter.

6 mm thick to increase their heat capacity, so that the temperature increase during a beam pulse not lead to an increase in its divergence by more than 1.2° (design value). To this end, all flanges onto which the IOS electrodes are mounted are water-cooled, which ensures complete heat dissipation between injector shots.

Accelerated ions enter the charge exchange chamber (neutralizer) as a beam (mixture of three main energy components). Fractional composition of the extracted ion beam (H^+, H_2^+, H_3^+) is determined by elementary processes in the plasma of the RF discharge. When fast ions pass through the neutralizer, as a result of the resonant charge exchange on the excess gas target, fast H_1^0 atoms of three different energies E, $E/2$, $E/3$ (E being main energy), respectively, are formed from fast ions H_1^+, H_2^+, H_3^+, and atoms with the energy $E/18$ ($E/10$) are formed from always existing impurity hydroxyl H_2O^+ ions for the hydrogen beam (D_2O^+ for deuterium). The neutralizer is a copper pipe (with 5 mm walls) 450 mm long and with an inner diameter of 197 mm, embedded in a double magnetic screen (pipe made of soft magnetic iron), which reduces the level of scattered magnetic fields below 0.3 G. Gas flows into the charge exchange chamber from the GDC source and is additionally puffed using a pulse solenoid valve. Total effective length of the neutralizer is 80 cm, and the pressure of the working gas in it is adjusted in such a way as to ensure equilibrium output of the beam's neutral component. [11] shows how the equilibrium yield of fast hydrogen atoms on an infinitely thick hydrogen target depends on the energy of particles. According to [11], the efficiency of hydrogen beam neutralization is approximately 50% for a component with the main energy (50 keV), 76% for a component with $E/2$, and 82% for a component with $E/3$.

At the output of the neutralizer, charged particles are removed from the beam using a deflecting electromagnet. The magnetic field in it is created by two coils (26 turns each) that are connected in series, placed in a hermetic case isolated from the vacuum volume. They cover an iron core. The magnetic field is created between the poles of the core, its intensity being up to 0.15 T at an up to 500 A current in coils. The strength of the electromagnetic field is selected depending on the type of gas and particle energy. The gap between

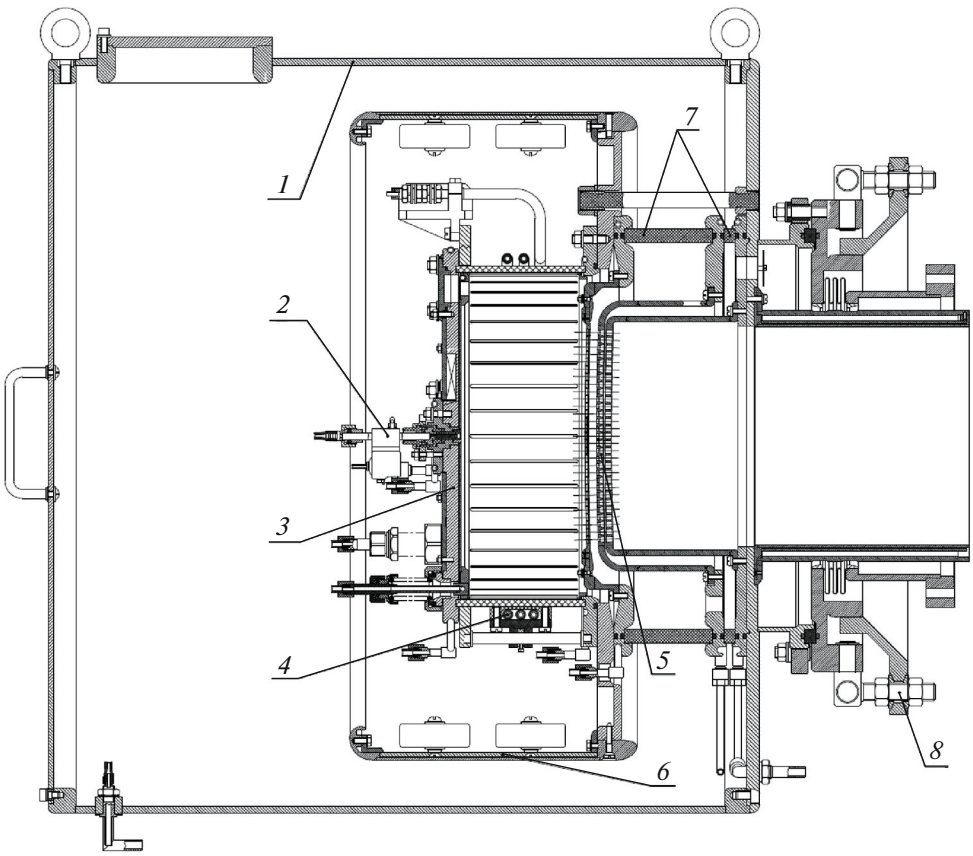

Fig. 2. Ion source: (*1*) external iron screen; (*2*) gas inlet valve and ignition device; (*3*) plasma chamber; (*4*) antenna; (*5*) IOS electrodes; (*6*) magnetic and electrostatic screen; (*7*) IOS ceramic insulators; (*8*) alignment device.

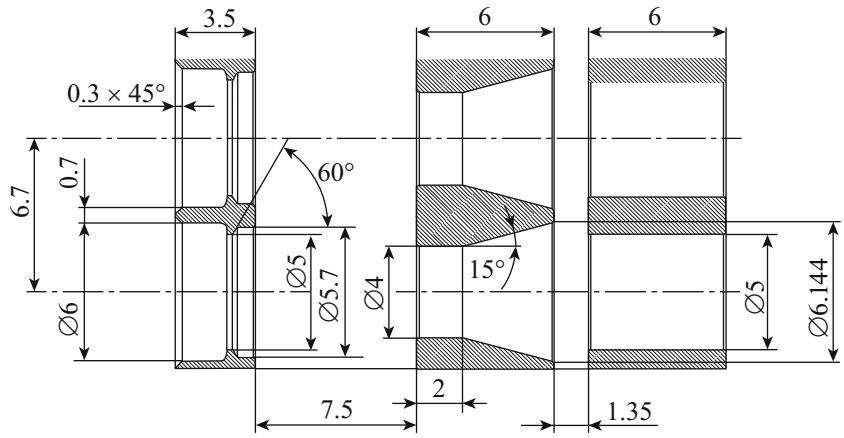

Fig. 3. Elementary cell geometry of the NBI-2 IOS.

the poles is 220 mm, and the width of the pole along the direction of the beam is 200 mm.

Remaining ions in the beam are deflected by the electromagnet onto the ion dump, which is a water-cooled V-shaped volume made of copper. The positioning and size of the ion dump are selected in such a way as to intercept all ions with three different energies.

As it moves along the beam path, the resulting atomic beam passes through the separating diaphragm and enters the aiming device. It serves to adjust the beam axis and is a copper disk with holes. Paired sec-

ondary emission detectors are located in the vertical and horizontal planes behind the holes. An alignment device is used to correct the direction of the beam axis in order to compensate for inaccuracies in the assembly of the ion source, particularly its IOS.

A movable absorbing calorimeter designed to control the parameters of the beam created by the injector is mounted at the output of the injector at a distance of approximately 2.5 m from the ion source. The absorber is brought onto the beam line in the injector testing mode or removed from it for the duration of the plasma experiment so that the neutral beam freely enter the tokamak. The calorimeter is a set of 11 water-cooled tubes arranged in the form of two wings (left and right), each carrying split thermocouples that measure the temperature of water-cooled tubes.

The vacuum volume of the injector and the tokamak chamber are connected by a specially designed docking unit which provides galvanic and mechanical decoupling and also cuts across the width of the beam. It includes a bushing insulator, bellows compensator, and water-cooled copper diaphragm (17 × 22 cm). The unit uses flanges to connect to the injector and the tokamak's inlet port.

The high-vacuum pumping system is built on the basis of Leybold TURBOVAC TMP 361 turbomolecular pump and Edwards GVSP30 fore-vacuum pump. The system maintains basic pressure level (up to 10^{-7} Torr) in the injector chamber. When the ion source is operational, the pressure in the injector volume increases due to pulsed puffing of the working gas. After leaving the neutralizer, the beam comprising fast atoms and ions continues to interact with the working gas flowing into the chamber. To minimize losses as the beam is transported into the tokamak, it is necessary to ensure the lowest possible gas pressure along its path. This is achieved by a large buffer volume of the injector chamber and two cryopumps installed on top of the injector's vacuum chamber. Each cryogenic pump in the molecular flow regime has the nominal pumping rate of 80×10^3 L/s for hydrogen. There are two branch pipes located on the pump flanges for filling the inner cryostat with liquid nitrogen. To cool cryopanels, the pumps use Sumitomo RDK-415D cryocooler with a W71C compressor, which ensures the cooling of the second stage to 3.5 K and ~20 K for the first stage. The cooling capacity of the first stage is not enough to ensure the protection from thermal radiation of chamber walls at room temperature and inner elements of the beam path which may have an even higher temperature, so an additional radiation shield cooled by liquid nitrogen is used. A cryoscreen panel made of copper with an area of 1.44 m^2 is attached to the second stage of the cryocooler and is placed between 1.13 m^2 copper chevron partition cooled by liquid nitrogen and copper screen attached to the first stage of the cryocooler. Total cooling power of the cryocooler is 60 W, and, taking into account the mass of its components, cooling the cryopump as a whole requires about 25 h. Standard consumption of liquid nitrogen is 3–4 L/h. Cryopumps are regenerated by warming up the cryostats with liquid nitrogen to room temperature and turning off cryocoolers. Gases released from cryopumps during regeneration are removed from the vacuum chamber by a turbomolecular pump.

The injector power supply system contains the following devices and blocks: high-voltage power source with active and passive injector breakdown protection devices; RF generator with anode power supply; power supply device for the second ion source grid; power supply device of the deflection electromagnet; power supply blocks of gas valves; power supply block for the ignition unit; and some other auxiliary power sources. The main feature of the injector's power supply system is that, when the injector is working, the body of the plasma chamber, along with the RF antenna, gas valve and the ignition unit, has high-voltage potential of up to 50 kV. The insulation voltage of these devices should be at least 60 kV. The power from the RF generator (up to 60 kW), its output cascade built on a powerful tetrode, is supplied to the antenna of the ion source through an isolation transformer. The voltage on the second grid is generated using an independent controlled source of negative voltage (up to −1000 V). The source of the injector's high-voltage power supply consists of a step-down multi-winding transformer and a set of 54 rectifiers with switches based on IGBT transistors, each transistor generating 1 kV output voltage. The rectifiers are powered by secondary windings of a three-phase 2 MW transformer. Half of the windings have the delta connection, and the other half have the star connection to reduce ripple levels. Primary windings of the transformer are powered by a three-phase 10 kV network.

The water cooling system is designed to remove heat from the injector's heat-stressed units and parts. It is built on the basis of a refrigeration unit with a closed primary circuit with distilled water. Two special pumps pump water to the injector components from a ~0.6 m^3 tank under the pressure of up to 6 atm.

The system for working gas puff is designed for measured gas supply to the GDC of the ion source and the neutralizer. It includes two pulse solenoid valves with gas flow limiting diaphragms; two buffer volumes (2 L each) filled with the working gas (hydrogen, deuterium) equipped with pressure gauges; and, respectively, two cylinders containing a supply of working gases and equipped with reducers. The working gas should have the highest possible degree of purification due to its direct impact on the purity of the beam injected into the tokamak, so the injector is outfitted with a system of valves designed to ensure prompt replacement of the working gas and vacuum pumping in the gas supply lines. When the injector is working, the GDC pulse valve is at high potential and is galvan-

ically isolated from buffer volumes. The pressure of the working gas in the buffer volumes is maintained at approximately 0.2 MPa.

The control and data acquisition system (CDAS) allows for remote control over technological processes associated with the setup and operation of the injector as a whole. It is built on the basis of an industrial computer with a specialized control program, galvanic isolation unit with digital-to-analog and analog-to-digital converters, digital inputs/outputs, and timing. The CDAS performs remote control and monitoring of injector subsystems, sets a time diagram of their operations, inputs voltage or current settings for the power supply systems, monitors blocking states, and automatically collects data on overall performance of injector systems.

FIRST ATOMIC INJECTOR UPDATE

In the Globus-M2 spherical tokamak, the toroidal magnetic field and plasma current are more than two times higher compared to Globus-M [12], which is expected to result in a significant increase in plasma density. To heat it efficiently, it is necessary to increase the energy of injected particles in order to ensure optimal depth of the atomic beam's penetration into the plasma before the particles' ionization. The update program for the neutral injection complex of the Globus-M tokamak included improvement of the existing atomic injector (NBI-1). A detailed description of its units and systems is given in [3]. Either the IPM-1 ion source (up to 1 MW power) or IPM-2 (up to 0.5 MW power) is installed in the NBI-1 depending on experimental needs. As part of the NBI-1 update, we developed a new IPM-3 three-electrode ion source. The difference between the IPM-3 and earlier IPM-1 and IPM-2 is in the design of a high-voltage insulator unit (HVIU) and slit ion-optical system. Still, the IPM-3 maintains the advantages of a plasma emitter with an arc discharge. The design specifications of the new ion source are shown in Table 2.

Table 2. IPM-3 design characteristics

Maximum power of the hydrogen ion beam, MW	2.4
Maximum beam pulse duration, ms	Up to 300
Beam divergence angle, degree:	
horizontal (*along the slits*)	No worse than ±0.6
vertical (*across the slits*)	No worse than ±1.5
Maximum ion beam current for hydrogen, A	60
Gas discharge chamber size, mm	200 × 330 × 130
Emission surface size, mm	120 × 250
Transparency of slit optics, %	No worse than 50
Negative electrode load current, A	Up to 7
Focal length in vertical and horizontal planes, m	3.0–3.5
Cathode current, A	1200
Cathode voltage, V	10.5
Discharge current, A	Up to 1300
Discharge voltage, V	Up to 70
Pause between pulses, s	No less than 120

The IOS of the new source consists of three multislit electrodes: emission electrode (EE), negative electrode (NE), and grounded electrode (GE). The EE closes the end of the GDC; the electric field created in the gap between the first pair of electrodes at the slits of the GDC forms a plasma emitter and extracts the ionic flow. The NE, being at a negative potential, ensures optimal focusing of individual ion beams that emerge from the EE slits and also blocks reverse flow of electrons from the secondary plasma. The third electrode is grounded to the injector case and ensures zero potential of the exiting ion beam. The HVIU is used to attach the IOS electrodes. The HVIU consists of three copper ring-shaped flanges connected to each other through ∅454 mm cylindrical ceramic insulators (80 and 15 mm tall) using textolite pins. The EE grids are mounted directly on the emission flange of the HVIU. The grids of the other two electrodes are installed inside the HVIU using metal stands mounted on the respective flanges. The layout drawing of the HVIU with attached IOS of the IPM-3 source is shown in Fig. 4.

To select electrode shapes, sizes of slits in and distances between them, we ran a simulation using the PBGUNS (Particle Beam GUN Simulation) program [13]. Calculations were made for maximum hydrogen beam parameters at an applied accelerating voltage of 40 kV. The optimal elementary cell geometry is shown in Fig. 5. The gap between the EE and NE is 6.0 mm; and the gap between the NE and GE is 1.5 mm. The optimal emission density of the current is approximately 4 mA/mm^2.

Each IOS electrode is made of five separate grids. For example, Fig. 6 shows one EE grid that is 120 mm tall and 50 mm wide. Thus, the total area of the emission surface is 120 × 250 mm^2. The working area of the EE grid is filled with 27 slits (3 × 38 mm each), so the total area of the emission slits is ~15.000 mm^2, which corresponds to 50% transparency. All grids are 3 mm thick. The EE grids are made of molybdenum of TsM2A grade, and the grids of the other two electrodes are made of chromium-zirconium bronze of BrKhTsr grade. We used water cooling channels to remove heat from the electrodes between pulses. Holes that are used to attach the grids to the electrodes on one side are designed to have the oval shape in order to compensate for thermal expansion during the injector shot. The working surface of the grids has cylindrical curvature along the slits; moreover, the NE

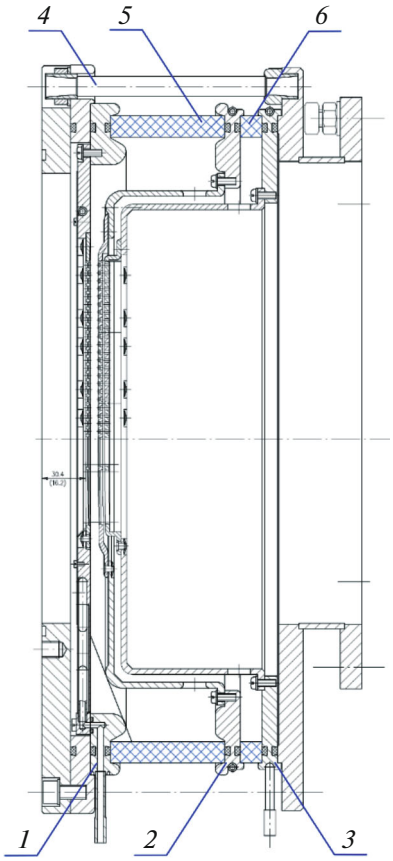

Fig. 4. HVIU assembled with IOS, cross section along (upper half) and across the slits (lower half): (*1*) EE flange, (*2*) NE flange, (*3*) GE flange, (*4*) textolite pins, (*5*) main ceramic insulator (50 kV), (*6*) secondary ceramic insulator (5 kV).

grids are displaced with respect to the EE grids that assure the focal distance of 3.0–3.5 m for the IOS. As we have indicated earlier, the optimal extractable current density in an elementary hydrogen beam is ~4 mA/mm^2 at the accelerating voltage of 40 kV, which yields a total ion current of 60 A given the IOS transparency.

The GDC of the new ion source is fully operational, and it has been tested by gradually increasing the discharge current from 250 A to approximately 1300 A (nominal value). The current–voltage characteristics of the arc discharge on hydrogen and deuterium are shown in Fig. 7.

The HVIU assembled with the IOS of the IPM-3 source is in its final production stage. For it to be fully operational, we added a step-up autotransformer to the high-voltage power supply system. The autotransformer allows us to expand the upper limit of obtained voltages' range to 40 kV [9]. A new gas puff system has been introduced into the GDC of the ion source (based on a piezoelectric valve). The system makes it possible to control the combustion mode of the arc discharge and the parameters of the plasma ion emitter in order to obtain the optimal shape, focusing, and power of the atomic beam [14]. We have updated probe diagnostics of the NBI-1 to increase the processing speed and accuracy for signals from the secondary emission probes, which significantly accelerated and simplified the optimization of the injected beam's parameters.

As time went by, the ion-optical system of the IPM-2 source failed to meet the design parameters, so we updated it. With the update, we achieved good vertical focusing, but horizontal focusing deteriorated because of the lack of curvature of the NE grids. The transverse dimensions of the beam on the calorimeter were 70 × 170 mm (at 90% power). Nevertheless, the total injected power of the deuterium beam was 500 kW, which meets the design parameters. Thus, the IMP-2 update made it possible to conduct neutral injection experiments on the Globus-M2 spherical tokamak [15].

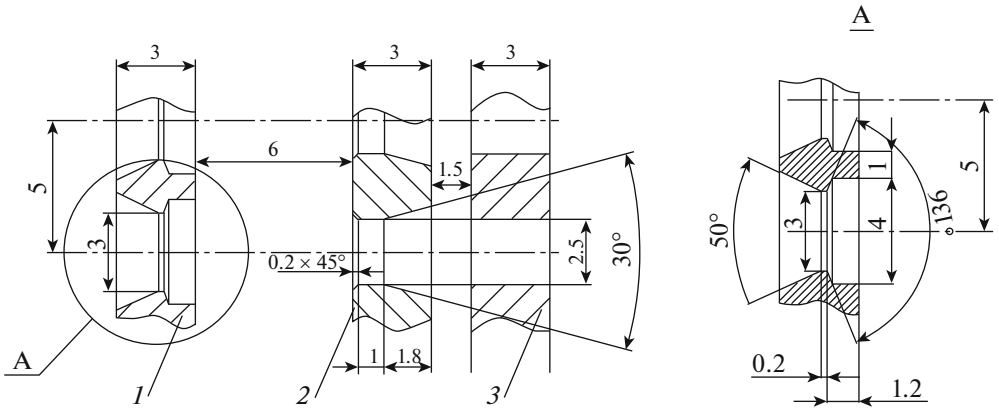

Fig. 5. Elementary cell geometry of IPM-3: (*1*) EE, (*2*) NE, (*3*) GE.

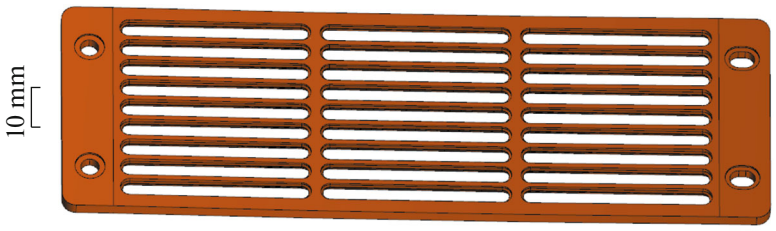

Fig. 6. 3D model of the EE grid.

SECOND ATOMIC INJECTOR COMMISSIONING AND ACHIEVING DESIGN PARAMETERS

At the first stage of preparing the NBI-2 for experiments, we analyzed possible injection geometry options and used them to develop experiment layout with introducing a second beam into the tokamak discharge (see Fig. 8). We decided to direct both atomic beams from the two injectors along the plasma current (co-injection). We chose the optimal injection geometry based on calculations of direct losses of fast particles for available impact parameter values (0.27–0.32 m) of the new injector. The calculations were made using a three-dimensional algorithm that tracks particle trajectories [16]. The inner wall of the receiving ports of the tokamak chamber opposite both injectors is lined with protective graphite tiles. For both injectors, the fast duration protection is organized, owing to which the beams are switched off almost instantly at the plasma discharge disruption.

At the maximum toroidal magnetic field of 1 T achievable in the Globus-M2 tokamak and 0.5 MA plasma current, the resulting direct losses were less than 5%, which is within the computational error for all available impact parameter values. Therefore, the impact parameter was optimized based on calculations in the reduced toroidal magnetic field of 0.7 T and 0.3 MA plasma current for two volume-averaged

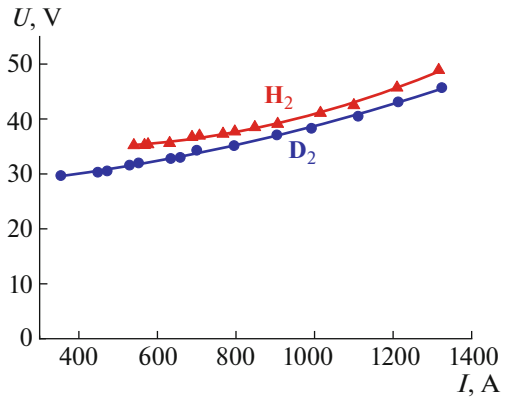

Fig. 7. Current–voltage characteristic of the arc discharge in the GDC of the IPM-3 source.

plasma density values (5.0×10^{19} and 1.0×10^{20} m^{-3}) at the injection energy of 40 keV. The results of this analysis are given in Fig. 9, which shows the dependence of fast particles' direct losses on possible impact parameter values of the second injector. Based on these calculations and taking into account design constraints, we set the impact parameter of the NBI-2 injector at 0.3 m.

At the second stage of preparations, we assembled the NBI-2 and all its auxiliary systems and installed it in the tokamak's experimental hall. We set up and tested the injector and ran high-voltage tests of power sources and components of the IOS injector, as well as vacuum and hydraulic tests of its components [17]. To ensure tangential injection of the NBI-2 atomic beam into the tokamak chamber, we outfitted its ∅0.4 m round port with an oblique pipe angled so as to ensure complete passage of the beam with the chosen impact parameter of 0.3 m. Then we connected the injector to the tokamak chamber through a vacuum valve using a docking unit that provided galvanic and mechanical decoupling and cut across the width of the beam to prevent it from touching the walls of the tokamak's inlet port.

At the final stage, we commissioned the NBI-2 and brought it to its design parameters. We obtained a beam of deuterium atoms with particle energy of 50 keV and 1.00 ± 0.05 MW power and measured its electrical characteristics (see Fig. 10), geometric dimensions, and the energy spectrum.

To measure the size of the beam and spatial distribution of its power over the cross section, we used the calorimeter. It is a set of water-cooled tubes arranged as two wings (left and right), each having a set of six spaced thermocouples that measure the temperature of the water-cooled tubes. Thermocouples are located symmetrically on each wing, five pieces in the vertical plane (one central and two thermocouples over and under it at a distance of 40 mm from each other) and one more in the horizontal plane (at a distance of 40 mm from the central one). The water flow passing through the calorimeter plates is known. Therefore, by integrating the surge of the signal from the thermocouples during the beam pulse, we get the value of thermal energy removed by the water. It is proportional to the beam power density locally incident on

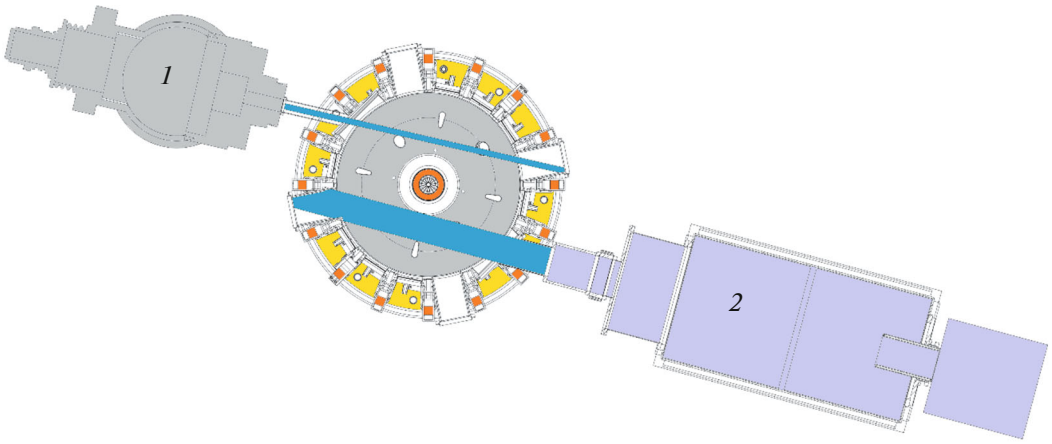

Fig. 8. Experimental layout on additional heating of the tokamak plasma using injectors (*1*) NBI-1 and (*2*) NBI-2.

the calorimeter tube located in front of the thermocouple. For example, Fig. 11 shows a typical graph of obtained temperature dependences over time from all thermocouples of the calorimeter's left wing, as well as the power profile of an 100 ms atomic beam and 1.35 MW electrical power (energy of beam particles is 50 keV; beam current is 27 A) calculated based on these data. Signal oscillograms of the beam are shown in Fig. 10.

For the accelerating voltage of 50 kV, after preliminary adjustment of voltage supplied to the second grid (−790 V), we performed scanning along the beam current (from 23 to 30 A). The experiments' results are given in Fig. 12, which shows the resulting dependence of the beam width at a $1/e$ power level of its current. Thus, the optimal deuterium beam current at 50 kV accelerating voltage was determined in the range of 25 to 27 A, whereas its width did not exceed 95 mm at the $1/e$ power level. Similar measurements were performed for the entire operating range of applied accelerating voltage of 30–50 kV in a wide span of beam currents for both hydrogen and deuterium injections. The results of the experiments are presented in Fig. 13. In the end, the width of the hydrogen and deuterium beams on the calorimeter does not exceed 110 mm at the $1/e$ power level for the entire operating range of applied accelerating voltage, and the beam power profile has a Gaussian shape.

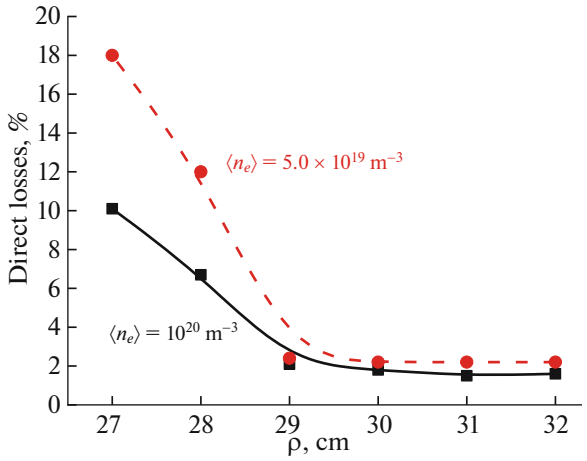

Fig. 9. Dependence of direct losses of fast particles with the energy of 40 keV on the impact parameter of the NBI-2 injector at $B_t = 0.7$ T and $I_p = 0.3$ MA for the case $\langle n_e \rangle = 5.0 \times 10^{19}$ (points and dashed line) and 1.0×10^{20} m^{-3} (squares and solid line).

For optimal focusing of the deuterium beam with 50 keV particle energy, we measured its energy spectrum using spectroscopic diagnostics of emission lines' Doppler shift. The measurement methodology is described in detail in [18]. To collect radiation generated as a result of the interaction of the injected beam's particles with the residual gas, the NBI-2 has a special port located on the calorimeter side. Using a lens with a fiber optic cable connected to its output, light is collected through this port towards the direction of the beam propagation. As we noted earlier, when a beam passes through a charge-exchange target in the neutralizer, fast D_1^0 atoms of three different E, $E/2$, $E/3$ energies (E being the main energy) are predominantly formed from fast D_1^+, D_2^+, D_3^+ ions, respectively. At the output of the neutralizer, the magnetic field removes charged particles from the beam. Atoms that remain in the beam are excited as a result of their collisions with the residual gas and emit the D_α line. When radiation is detected, five lines are observed: one corresponds to the unshifted D_α line from the residual gas; three other lines, strongly shifted as a result of the Doppler effect, correspond to particles with v, $v/\sqrt{2}$, $v/\sqrt{3}$ velocities ($v = \sqrt{2E}/M$, where M is the mass of beam particles); and one line corresponds to impurity additives that typically have

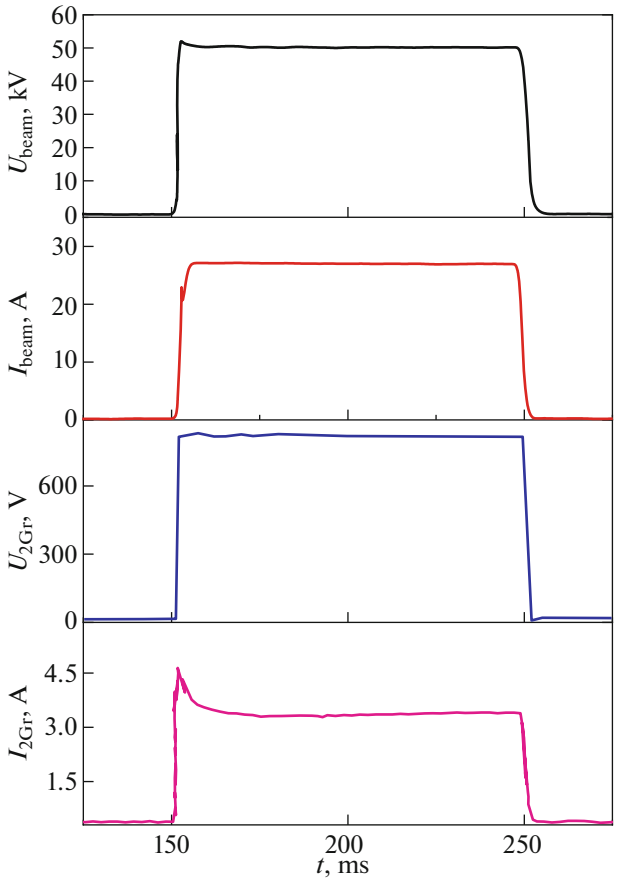

Fig. 10. Oscillograms of the main signals of the NBI-2 power supply system during the 100 ms deuterium beam shot, where U_{beam} is the applied accelerating voltage; I_{beam} is the total current of the ion beam; U_{2Gr} is the negative voltage of the second grid; I_{2Gr} is the load current of the second grid.

$E/10$ energy. This radiation is collected by a fiber optic spectrometer. The optical method of determination is very convenient (the main advantage is that it is non-contact), since it makes it possible to determine the composition of the beam directly during the plasma experiment. An example of the emission spectrum for a deuterium beam with $E = 50$ keV (100 ms exposure time) is shown in Fig. 14. We processed and analyzed the resulting energy spectrum. Our analysis showed that 36% of the transferred current's relative fraction in the atomic beam belongs to the component with the main energy, 40%—to the component with the $E/2$ energy, 22%—to the component with the $E/3$ energy, and 2% to the component with the $E/10$ energy.

The power of the atomic beam P_{nb} at the injector output is the sum of the powers of the three main components with their respective E, $E/2$, $E/3$ energies and the impurity component with the energy of $E/10$. P_{nb} can be approximately calculated from the known power of the ion beam $P_{ib} = U_{beam}I_{beam}$, which is 1.35 MW for the deuterium beam in the injector operating mode shown in Fig. 10. In this case, it is necessary to account for losses from the conversion of the ion beam into the atomic beam in the charge exchange chamber η_{io}, as well as losses from transporting and cutting off a part of the beam by the injector diaphragms η_{tr}. As a result,

$$P_{nb} = \eta_{io}\eta_{tr}P_{ib}.$$

Parameter η_{tr} depends on focusing, alignment of the beam axis with the injector line, and reionization losses (i.e., depends on the vacuum conditions along the atomic beam path) and is 0.85–0.95. Parameter η_{io} is determined by cross sections of atomic processes in the neutralizer; depends on the energy of ions and, consequently, on the components that make up the ion beam taking into account different efficiency of components' neutralization, as well as the optimally selected "optical" thickness of the gas target; and is 0.5–0.8 (at $U_{beam} = 20$–50 kV). For a component with the main energy (50 keV) of the deuterium beam D^+, the neutralization coefficient is 76%; for the component with $E/2$, D_2^+—84%; for the component with

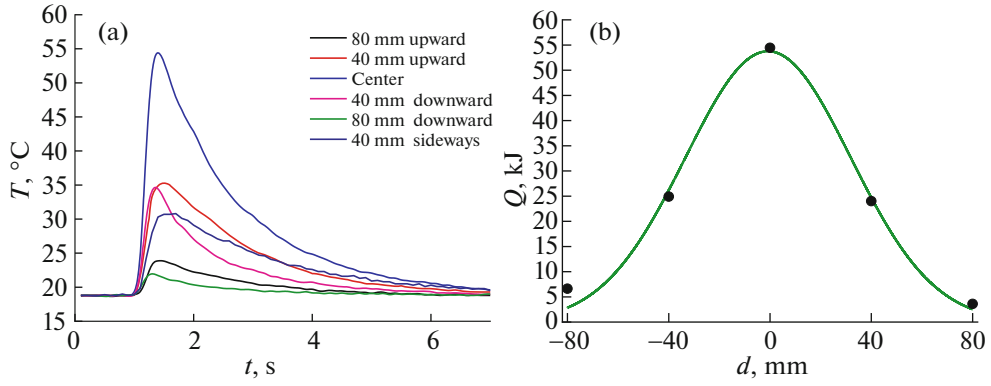

Fig. 11. (a) Temperature dependence over time from thermocouples of the left-hand wing of the calorimeter and (b) atomic beam power profile calculated on the basis of these data.

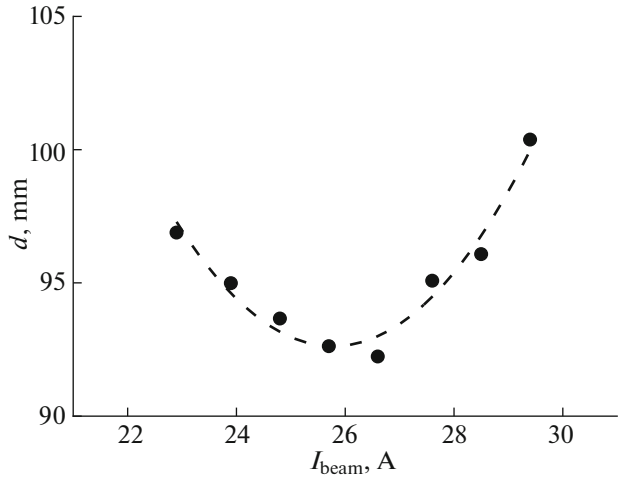

Fig. 12. Dependence of the beam diameter over the $1/e$ power level on its current.

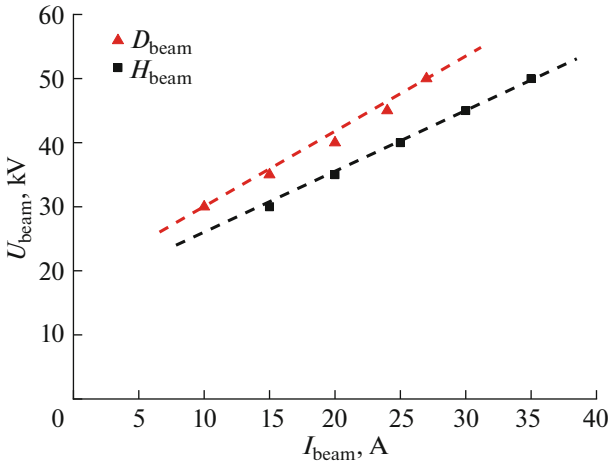

Fig. 13. Dependence of the optimal beam current on the applied accelerating voltage of the NBI-2.

$E/3$, D_3^+—87%; and for the component with $E/10$, D_2O^+—92% [11]. The component composition of the ion beam (i.e., relative fractions of the transferred current by each of its components) is determined using the Doppler shift spectroscopy. For the 50-keV deuterium beam $D^+ : D_2^+ : D_3^+ : D_2O^+ = 0.39 : 0.40 : 0.22 : 0.02$ at the optimal ion current of 27 A. Thus, the component D^+ takes 9.7 A, D_2^+—10.8 A, D_3^+—5.9 A, D_2O^+—0.6 A. Taking into account different equilibrium neutralization coefficients for each energy component of the ion beam, we get the following parameter:

$$\eta_{io} = 0.36 \times 0.76 + 0.40 \times 0.84 + 0.22 \times 0.87 + 0.02 \times 0.92 = 0.82.$$

Thus, the power of 50 keV deuterium beam at the output of the injector is 1.00 ± 0.05 MW.

EXPERIMENT RESULTS ON HEATING GLOBUS-M2 TOKAMAK PLASMA BY TWO ATOMIC BEAMS

In accordance with the selected layout (Fig. 8), we carried out a series of experiments on additional heating of the Globus-M2 tokamak deuterium plasma with two deuterium beams of the NBI-1 and NBI-2. The plasma of the device had a divertor configuration, the displacement of the center of the external magnetic surface along the major radius with respect to the geometric center of the chamber was 2 cm, B_t was 0.9 T, and I_p was 0.4 MA. The neutral beam of NBI-2 with 0.95 MW power and 46 keV particle energy was turned on for 150 ms of the discharge at the stage of the increasing plasma current, whereas the total power flow through the plasma boundary gradually increased, which led to the L–H transition. The NBI-1 deuterium beam with 0.5 MW power and 28 keV particle energy was injected for the 180 ms of the discharge at the plateau stage of the plasma current, which caused a strong increase in the ion temperature, and, consequently, an increase in the energy stored in the plasma. At the start of the NBI-1, average plasma density was 5×10^{19} m^{-3}. Figure 15 shows spatial distributions of electron and ion temperatures, as well as electron density profile measured in the discharge No. 42416 in the equatorial plane of the tokamak. The ion temperature measured using the CXRS diagnostics [19] along the emission line of a 5x-ionized impurity ion of carbon C^{5+} (the emission wavelength $\lambda_0 = 5290.525$ Å) agrees with the data of active NPA diagnostics [20], its measurements localized in the area where the NBI-1 beam intersects with the NPA observation line. Both diagnostics demonstrate an increase in the ion temperature to 4 keV when the second beam is injected. The electron temperature on

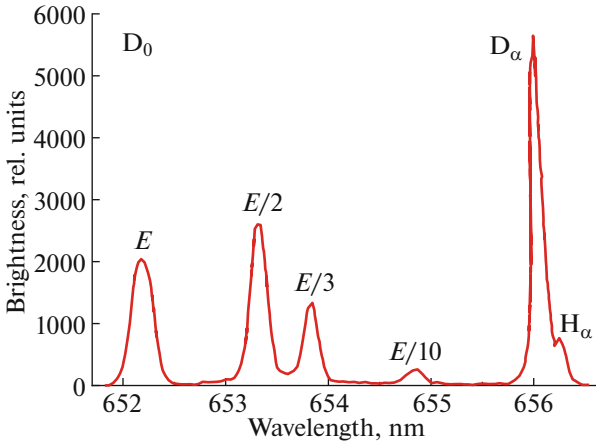

Fig. 14. Emission spectrum of a deuterium atomic beam with the main particle energy $E = 50$ keV.

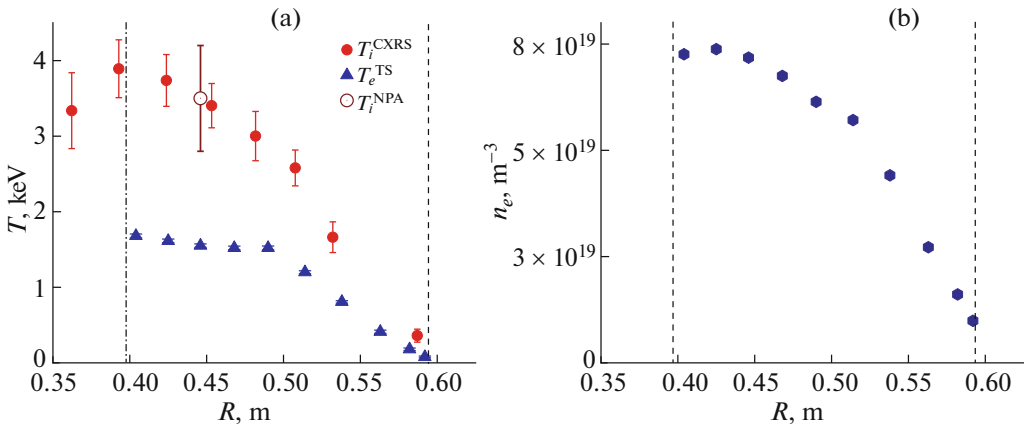

Fig. 15. (a) Spatial distributions of electron and ion temperatures, (b) electron density profile measured at 192 ms of the discharge no. 42416 at $B_t = 0.9$ T and $I_p = 0.4$ MA with deuterium injection (NBI-1: 0.5 MW power, 28 keV energy; NBI-2: 0.95 MW power, 46 keV energy). The vertical line on the left corresponds to the magnetic axis position, and that on the right to the last closed magnetic surface.

the plasma axis measured with Thomson scattering (TS) diagnostics [21] does not exhibit any major changes and remains at the level of 1.5 keV throughout the entire NBI-1 shot, while plasma density increases significantly. CXRS diagnostic data show that the injection of neutral beams into the plasma gives it a significant torque, whereby the toroidal rotation rate of plasma in the discharge No. 42416 reaches 140 km/s in the near-axis region.

CONCLUSIONS

We upgraded the neutral injection complex of the Globus-M2 tokamak by adding the second NBI-2 and improving the existing NBI-1.

For the NBI-1, we developed a new IPM-3 three-electrode ion source. The difference between the IPM-3 and the earlier IPM-1 and IPM-2 lies in the design of a high-voltage insulator assembly and slit ion-optical system, but the IPM-3 still has the advantages of a plasma emitter with an arc discharge. The IPM-3 allows for the injection of beam atoms with up to 40 keV energy and up to 1 MW power into the tokamak plasma. The HVIU assembled with the IOS of the IPM-3 source is currently at the final production stage, and its GDC is fully prepared for operation. At the same time, the ion-optical system of the IPM-2 source was updated, which allowed for good beam focusing. Its transverse dimensions at the beam receiver/calorimeter were 70 × 170 mm (at 90% power level), and the total injected power of the deuterium beam reached 0.5 MW.

For the NBI-2, we analyzed possible injection geometry options and used them to develop experimental layout with introducing a second beam into the tokamak discharge. We decided to direct both atomic beams from two injectors along the plasma current (co-injection). Based on the calculations of direct losses of fast particles and taking into account design constraints, we selected 30 cm as the impact parameter of the NBI-2. In accordance with the selected experimental setup, the NBI-2 and all its auxiliary systems were assembled and mounted in the experimental hall of the tokamak. They were adjusted and tested. The NBI-2 was docked to the tokamak chamber. We performed commissioning by bringing the NBI-2 to its design parameters. We obtained a beam of deuterium atoms with 50 keV energy of particles and measured the beam's electrical characteristics. For this beam, we selected the optimal current (27 A) that corresponds to its minimum geometric dimensions (no more than 95 mm at the $1/e$ power level) and the best focusing. Using spectroscopic diagnostics for the focused deuterium beam with 50 keV particle energy, we measured the energy spectrum and used it to calculate the beam power on the calorimeter, which was 1.00 ± 0.05 MW. We also measured the optimal beam current over the entire operating range of 30–50 kV applied accelerating voltage for hydrogen and deuterium injection. The diameter of the hydrogen and deuterium beams on the calorimeter does not exceed 110 mm at the $1/e$ power level throughout the entire operating range of the applied accelerating voltage, and the beam power profile has a Gaussian shape.

Thus, we put into operation and brought to design parameters a new high-energy atomic injector capable of generating a beam of hydrogen or deuterium atoms with up to 50 keV particle energy at up to 1 s pulse duration in order to perform experiments on additional plasma heating using the Globus-M2 device

In experiments on additional heating of the Globus-M2 tokamak plasma by injecting two NBI-1 and NBI-2 atomic beams, we obtained a stable reproducible operation mode with high ion temperature T_i in

the order of 4 keV, which significantly exceeds the electron temperature T_e of 1.5 keV. This achievement made it possible to approach the range of experimental parameters that are typical for a thermonuclear reactor.

ACKNOWLEDGMENTS

The study was carried out at the Unique Scientific Facility "Spherical Globus-M tokamak," which is a part of the Federal Center for Collective Use "Materials Science and Diagnostics in Advanced Technologies" of the Ioffe Institute.

FUNDING

Research in the "Second Atomic Injector Commissioning and Achieving Design Parameters" Section are supported by the State Assignment (0040-2019-0023). The development of a new IPM-3 three-electrode IOS ion source was supported in part by the Ministry of Science and Higher Education of the Russian Federation under the State Assignment (research project code FWGM-2022-0016). Experiments with the injection of two atomic beams into the Globus-M2 tokamak plasma were supported by the State Assignment (0034-2021-0001).

CONFLICT OF INTEREST

The authors of this work declare that they have no conflicts of interests.

REFERENCES

1. V. B. Minaev, V. K. Gusev, N. V. Sakharov, V. I. Varfolomeev, N. N. Bakharev, V. A. Belyakov, E. N. Bondarchuk, P. N. Brunkov, F. V. Chernyshev, V. I. Davydenko, V. V. Dyachenko, A. A. Kavin, S. A. Khitrov, N. A. Khromov, E. O. Kiselev, et al., Nucl. Fusion **57**, 066047 (2017). https://doi.org/10.1088/1741-4326/aa69e0
2. V. K. Gusev, V. E. Golant, E. Z. Gusakov, V. V. D'yachenko, M. A. Irzak, V. B. Minaev, E. E. Mukhin, A. N. Novokhatskii, K. A. Podushnikova, G. T. Razdobarin, N. V. Sakharov, E. N. Tregubova, V. S. Uzlov, O. N. Shcherbinin, V. A. Belyakov, et al., Tech. Phys. **44**, 1054 (1999). https://doi.org/1 10.1134/1.1259469
3. V. K. Gusev, A. V. Dech, L. A. Esipov, V. B. Minaev, A. G. Barsukov, G. B. Igon'kina, V. V. Kuznetsov, A. A. Panasenkov, M. M. Sokolov, G. N. Tilinin, A. V. Lupin, and V. K. Markov, Tech. Phys. **52**, 1127 (2007). https://doi.org/10.1134/S1063784207090058
4. W. W. Heidbrink and G. J. Sadler, Nucl. Fusion **34**, 535 (1994). https://doi.org/10.1088/0029-5515/34/4/I07
5. G. S. Kurskiev, I. V. Miroshnikov, N. V. Sakharov, V. K. Gusev, Yu. V. Petrov, V. B. Minaev, I. M. Balachenkov, N. N. Bakharev, F. V. Chernyshev, V. Yu. Goryainov, A. A. Kavin, N. A. Khromov, E. O. Kiselev, S. V. Krikunov, K. M. Lobanov, et al., Nucl. Fusion **62**, 104002 (2022). https://doi.org/10.1088/1741-4326/ac881d
6. C. C. Petty, M. R. Wade, J. E. Kinsey, R. J. Groebner, T. C. Luce, and G. M. Staebler, Phys. Rev. Lett. **83**, 3661 (1999). https://doi.org/10.1103/PhysRevLett.83.3661
7. A. Fasoli, C. Gormenzano, H. L. Berk, B. Breizman, S. Briguglio, D. S. Darrow, N. Gorelenkov, W. W. Heidbrink, A. Jaun, S. V. Konovalov, R. Nazikian, J. M. Noterdaeme, S. Sharapov, K. Shinohara, D. Testa, et al., Nucl. Fusion **47**, S264 (2007). https://doi.org/10.1088/0029-5515/47/6/S05
8. D. J. Schlossberg, G. R. McKee, R. J. Fonck, K. H. Burrell, P. Gohil, R. J. Groebner, M. W. Shafer, W. M. Solomon, and G. Wang, Phys. Plasmas **16**, 080701 (2009). https://doi.org/10.1063/1.3192766
9. P. B. Shchegolev, V. B. Minaev, A. Yu. Telnova, N. N. Bakharev, P. R. Goncharov, V. K. Gusev, G. S. Kurskiev, I. V. Miroshnikov, M. I. Patrov, Yu. V. Petrov, N. V. Sakharov, I. V. Shikhovtsev, and S. Yu. Tolstyakov, J. Phys.: Conf. Ser. **907**, 012013 (2017). https://doi.org/10.1088/1742-6596/907/1/012013
10. A. Sorokin, V. Belov, V. Davydenko, P. Deichuli, A. Ivanov, A. Podyminogin, I. Shikhovtsev, G. Shulzhenko, N. Stupishin, and M. Tiunov, Rev. Sci. Instrum. **81**, 02B108 (2010). https://doi.org/10.1063/1.3266141
11. N. N. Semashko, A. N. Vladimirov, V. V. Kuznetsov, V. M. Kulygin, and V. V. Panasenkov, *Injectors of Fast Hydrogen Atoms* (Energoizdat, Moscow, 1981) [in Russian].
12. N. N. Bakharev, I. M. Balachenkov, F. V. Chernyshev, I. N. Chugunov, V. V. Dyachenko, V. K. Gusev, M. V. Iliasova, E. M. Khilkevitch, N. A. Khromov, E. O. Kiselev, A. N. Konovalov, G. S. Kurskiev, V. B. Minaev, A. D. Melnik, I. V. Miroshnikov, et al., Plasma Phys. Rep. **46**, 675 (2020). https://doi.org/10.1134/S1063780X20070016
13. J. E. Boers, in *Proceedings of the 1995 Particle Accelerator Conference* (IEEE, New York, 1995), p. 2312.
14. A. Y. Telnova, V. B. Minaev, P. B. Shchegolev, D. V. Razumenko, G. S. Kurskiev, and A. V. Lupin, Tech. Phys. **62**, 1112 (2017). https://doi.org/10.1134/S1063784217070246
15. A. Yu. Telnova, V. B. Minaev, A. A. Panasenkov, and P. B. Shchegolev, Tech. Phys. **67** (4), 449 (2022). https://doi.org/10.21883/TP.2022.04.53600.292-21
16. N. N. Bakharev, F. V. Chernyshev, P. R. Goncharov, V. K. Gusev, A. D. Iblyaminova, V. A. Kornev, G. S. Kurskiev, A. D. Melnik, V. B. Minaev, M. I. Mironov, M. I. Patrov, Yu. V. Petrov, N. V. Sakharov, P. B. Shchegolev, S. Yu. Tolstyakov, et al., Nucl. Fusion **55**, 043023 (2015). https://doi.org/10.1088/0029-5515/55/4/043023
17. A. Yu. Telnova, V. B. Minaev, P. B. Shchegolev, N. N. Bakharev, I. V. Shikhovtsev, and V. I. Varfolomeev, J. Phys.: Conf. Ser. **1400**, 077015 (2019). https://doi.org/10.1088/1742-6596/1400/7/077015

18. P. B. Shchegolev, V. B. Minaev, and I. V. Miroshnikov, Nauchno-Tech. Vedomosti S.-Peterb. Gos. Polotekh. Univ. Fiz.-Mat. Nauki, No. 4 (158), 79 (2012).

19. Yu. V. Petrov, P. A. Bagryansky, I. M. Balachenkov, N. N. Bakharev, P. N. Brunkov, V. I. Varvalomeev, A. V. Voronin, V. K. Gusev, V. A. Goryainov, V. V. Dyachenko, N. V. Ermakov, E. G. Zhilin, N. S. Zhiltsov, S. V. Ivanenko, M. V. Il'yasova, et al., Plasma Phys. Rep. **49**, 1459 (2023).

20. N. N. Bakharev, I. M. Balachenkov, F. V. Chernyshev, V. K. Gusev, E. O. Kiselev, G. S. Kurskiev, A. D. Melnik, V. B. Minaev, M. I. Mironov, V. G. Nesenevich, Yu. V. Petrov, N. V. Sakharov, P. B. Shchegolev, O. M. Skrekel, A. Yu. Telnova, et al., Plasma Phys. Controlled Fusion **63**, 125036 (2021). https://doi.org/10.1088/1361-6587/ac3497

21. G. S. Kurskiev, N. S. Zhiltsov, A. N. Koval, A. F. Kornev, A. M. Makarov, E. E. Mukhin, Yu. V. Petrov, N. V. Sakharov, V. A. Solovey, E. E. Tkachenko, S. Yu. Tolstyakov, and P. V. Chernakov, Tech. Phys. Lett. **48** (15), 78 (2022). https://doi.org/10.21883/TPL.2022.15.54273.19019